



Influence of Viscosity on Dynamic Magnetization of Thermally Blocked Iron Oxide Nanoparticles Characterized by a Sensitive AC Magnetometer

Mohd Mawardi Saari¹ · Nazatul Shareena Suhaimi¹ · Mohd Herwan Sulaiman¹ · Nurul Akmal Che Lah² · Kenji Sakai³ · Toshihiko Kiwa³ · Keiji Tsukada³

Received: 8 May 2018 / Accepted: 16 January 2019 / Published online: 2 February 2019
© Springer Science+Business Media, LLC, part of Springer Nature 2019

Abstract

In this work, we show that the viscosity of carrier liquid affects the dynamic magnetization of thermally blocked multi-core iron oxide nanoparticles. The core size of the nanoparticles was determined from the magnetization curve measured by a specially developed high- T_c SQUID magnetometer and calculated to be 11.7 nm. Using an AC magnetometer developed based on induction coils, the dynamic magnetization of the multi-core iron oxide nanoparticle solution was measured from 3 Hz to 10.48 kHz. Later, we reconstructed of the hydrodynamic size distribution of the particles by assuming a log-normal distribution of particle size in an AC susceptibility model by Shliomis and Stepanov, which accounts for anisotropic directions of the easy axes of magnetic nanoparticles with respect to the excitation field direction. The reconstructed hydrodynamic sizes showed an average diameter of 130 nm and agreed with the size determined by dynamic light scattering method. In the case of increasing viscosity of the carrier liquids from 0.89 to 8.11 mPa s, the dynamic magnetization peaks of the imaginary component have shifted to a lower frequency region. We showed that the harmonics ratio and phase delay upon the magnetic field excitation at 30 Hz could also be used to determine the viscosity of carrier liquid independently.

Keywords Brownian relaxation · Dynamic magnetization · Iron oxide nanoparticles · Magnetometer

1 Introduction

Magnetic nanoparticles (MNPs) have received significant interest recently, mainly owing to their size of being able to interact with their environment at the nanometer scale, and their high signal-to-noise ratio of detection using the magnetic method. MNPs have been utilized in the in vivo imaging as a contrast agent in magnetic resonance imaging (MRI) technique [1] and recently, as a tracer in an emerging tomographic imaging modality called magnetic particle imaging (MPI)

technique [2–7]. Since their non-linear magnetic signal is one type of transparent to biological tissues, MPI shows a promising clinical application owing to its high temporal and spatial resolutions compared to other imaging techniques. In fact, MNPs' intrinsic magnetic characteristics and their environmental interaction are commonly utilized in biomedical applications such as exploiting their heat generation at a high frequency in magnetic hyperthermia [8, 9] and magnetic relaxation in magnetic immunoassays [10]. Moreover, it was also reported that MNPs enable a sensitive viscosity determination of their suspension liquid [11]. On the whole, MNPs are preferable and have been employed in a wide range of applications through the exploitation of their dynamics magnetization which is strongly depended by the effects of the particle size, morphology, intrinsic magnetic properties, and environmental interaction (e.g., viscosity and hydrodynamic size). Therefore, clarification on these factors is essential so that MNPs can be tailored for intended applications [12].

The magnetic characterization of the MNPs can be achieved from the DC and AC susceptibility [13] methods apart from magnetic relaxation [14] and remanence methods. The AC susceptibility measurement can provide the information of size

✉ Mohd Mawardi Saari
mmawardi@ump.edu.my

¹ Faculty of Electrical & Electronic Engineering, Universiti Malaysia Pahang, Pekan Campus, 26600 Pekan, Pahang, Malaysia

² Innovative Manufacturing, Mechatronics and Sports Lab (iMAMs), Faculty of Manufacturing Engineering, Universiti Malaysia Pahang, Pekan Campus, 26600 Pekan, Pahang, Malaysia

³ Graduate School of Interdisciplinary Science and Engineering in Health Systems, Okayama University, Okayama 700 8530, Japan

distribution, harmonics, and magnetic anisotropy with a fast response to the measurement by observing Neel and Brownian relaxations [15]. The DC susceptibility could also provide the size distribution of the MNP's core [16, 17]. To evaluate and serve as one of the methods for the standardization of MNPs, we have reported specially designed DC and AC magnetometers [18, 19]. In this work, using the developed magnetometers, the investigation on the dynamics of a commercial ferromagnetic multi-core iron oxide nanoparticles at a different viscosity of carrier liquids is performed. Later, the distribution of magnetic moment is constructed based on the measured magnetization curve. The hydrodynamic size of the particles is determined from the AC susceptibility model proposed by Shliomis and Stepanov [20], which includes an inter-potential- and intra-potential-well contribution to the magnetic response. The measurements on the harmonic profile of MNPs at the different intensity of AC magnetic fields are presented. Also, the viscosity of carrier liquids that is estimated from the imaginary part of the dynamic magnetization, ratio, and lagging phase of the odd harmonics even at the different intensity of the AC excitation fields are also demonstrated.

2 Methodology

2.1 AC Magnetometer

The AC magnetometer used in this work has been specially developed for characterization of MNPs [19]. Briefly, the AC magnetometer is mainly composed of the excitation and detection units. In the excitation unit, an excitation coil is resonated by a capacitor network to reduce the impedance of the excitation coil at the high-frequency region. The capacitor network is fabricated to resonate the excitation coil at discrete frequencies on a logarithmic scale. The 300-turn excitation coil is fabricated from a Litz wire and designed to achieve a high homogeneity and efficiency of the excitation field [21]. In the detection unit, a first-order axial differential coil is used as the detection sensor. The first-order differential coil is composed of two identical 1000-turn coils, whose inner diameter and baseline are 15 mm and 23 mm, respectively. The attenuation of the direct feedthrough is achieved by manually tuning the position of the detection coil relative to the excitation coil. The signal from the detection coil is lock-in detected using a lock-in amplifier (LI5640, NF Corporation) for a phase-sensitive detection.

2.2 AC Susceptibility Model

Shliomis and Stepanov proposed that for an ensemble of MNPs with randomly distributed easy axes, the complex AC susceptibility in response to the applied AC magnetic field is given by [20, 22, 23]:

$$\chi = \frac{1}{3} \left(\frac{\chi_{\parallel}}{1 + i\omega\tau_{\parallel}} + 2\chi_{\perp} \right). \quad (1)$$

Here, $\omega = 2\pi f$, χ_{\parallel} , χ_{\perp} , and τ_{\parallel} are the angular frequency, the susceptibilities for particles with easy axes parallel and perpendicular to the applied AC field, and the parallel component of relaxation time. The parallel and perpendicular components of susceptibilities are expressed by $\chi_{\parallel} = \frac{\mu_0 M_s^2 V_c}{k_B T} \frac{R'}{R}$ and $\chi_{\perp} = \frac{\mu_0 M_s^2 V_c}{k_B T} \frac{R - R'}{2R}$ with $R(\sigma) = \int_0^1 e^{\sigma x^2} dx$ and $R'(\sigma) = \int_0^1 x^2 e^{\sigma x^2} dx$. Here, μ_0 is the vacuum permeability, M_s is the saturation magnetization of MNP, V_c is the core volume of MNP, and $\sigma = KV_c/k_B T$ is the dimensionless ratio between the anisotropy energy KV_c and thermal energy $k_B T$. In the large barrier range where the magnetic moment is thermally blocked, $\sigma \gg 1$, χ_{\perp} reaches the independent temperature value $\mu_0 M_s^2 / 2K$ whereas $\chi_{\parallel} \approx \mu_0 M_s^2 V_c / k_B T - \mu_0 M_s^2 / K$ [22]. In this large barrier, Eq. (1) can be rewritten by,

$$\chi = \chi_0 \left(\frac{\sigma - 1}{\sigma} \frac{1}{1 + i\omega\tau_{\parallel}} + \frac{1}{\sigma} \right), \quad (2)$$

where static susceptibility $\chi_0 = \mu_0 M_s^2 V_c / 3k_B T$. It should be noted that the expression given in Eq. (2) is similar to equation in the reference [24] where the second term in the right-hand side stands for the intra-potential-well contribution, which is in contrast to the standard Debye model given by $\chi = \chi_0 / (1 + i\omega\tau)$.

Furthermore, $\tau_{\parallel}^{-1} = \tau_l^{-1} + \tau_B^{-1}$ represents the effective relaxation time of longitudinal Neel and Brownian relaxation times, where they are given by $\tau_l = \tau_0 \sqrt{\pi} e^{\sigma} / 2\sigma^{3/2}$ ($\sigma \geq 2$) and $\tau_B = 3V_H \eta / k_B T$, respectively. Here, τ_0 is the intrinsic relaxation time related to intra-potential-well dynamics (typically of the order 10^{-9} s [24]), V_H is the hydrodynamic volume of MNPs, and η is the viscosity of carrier liquid. In the case where $\tau_B \ll \tau_l$, i.e., thermally blocked MNPs, and the hydrodynamic diameter D_H described by a log-normal distribution $f(D_H) = \exp\left(-(\ln(D_H/D_0))^2 / 2\delta_D^2\right) / \sqrt{2\pi} D_H \delta_D$, the dynamic susceptibility of multi-core MNPs can be expressed by,

$$\chi = \chi_0 \left(\frac{\sigma - 1}{\sigma} \int_0^{\infty} \frac{f(D_H) dD_H}{1 + i\omega\tau_B} + \frac{1}{\sigma} \right), \quad (3)$$

where D_0 and δ_D are the median and dimensionless parameter related to the standard deviation. The average diameter and standard deviation of D_H are given by $D_0 \exp(\delta_D^2/2)$ and $D_0 \exp(\delta_D^2/2) \sqrt{\exp(\delta_D^2) - 1}$. In this work, we assume that σ and χ_0 can be approximated by the average ratio of anisotropy and thermal energies $\langle\sigma\rangle$, and average static susceptibility $\langle\chi_0\rangle$ for multi-core particles [15]. Then, the real χ' and imaginary parts χ'' of the susceptibility can be expressed by,

$$\chi' = \langle \chi_0 \rangle \left(\frac{\langle \sigma \rangle - 1}{\langle \sigma \rangle} \int_0^\infty \frac{f(D_H) dD_H}{1 + (\omega\tau_B)^2} + \frac{1}{\langle \sigma \rangle} \right), \tag{4}$$

$$\chi'' = \langle \chi_0 \rangle \left(\frac{\langle \sigma \rangle - 1}{\langle \sigma \rangle} \int_0^\infty \frac{\omega\tau_B f(D_H) dD_H}{1 + (\omega\tau_B)^2} \right). \tag{5}$$

It should be noted that Eqs. (4) and (5) are almost similar to equations derived in references [24, 25]; however, $\langle \sigma \rangle$ and $\langle \chi_0 \rangle$ were used instead of individual values of particles and the high frequency susceptibility χ_∞ in reference [25] could be estimated using the relation between the first and second terms of Eq. (4) even in a narrowband frequency measurement range.

2.3 Sample Preparation

The commercial multi-core iron oxide nanoparticle used in this study was nanomag®-D (Micromod Partikeltechnologie GmbH) with a typical diameter of 130 nm. The five sets of the different carrier liquid viscosity were prepared by varying the weight of glycerol mixed in a constant volume of purified water from 0 to 80 wt/V %. Then, 200 μ l of stock suspension of the particles was diluted in 1 ml of the prepared carrier liquids. The dynamic magnetization with respect to excitation frequency was measured using the developed AC magnetometer [19] from 3 Hz to 10.48 kHz at a constant amplitude of 2.6 mT. The response characteristic at different amplitudes of the excitation field was measured at 30 Hz from 1.3 to 7.8 mT.

3 Result and Discussion

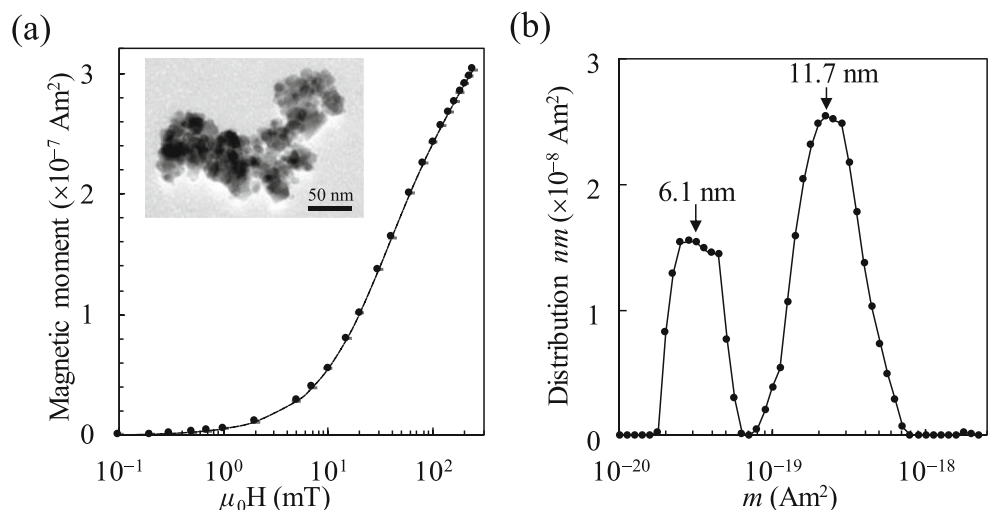
3.1 The Distribution of Core and Hydrodynamic Sizes

Fig. 1 a shows the initial magnetization curve measured by the high- T_c SQUID magnetometer from 0.1 to 240 mT. From the

magnetization curve, the distribution of magnetic moment is constructed as shown in Fig. 1 b. Details on the distribution construction can be found in references [18, 26]. The highest peak corresponding to a core size of 11.7 nm, was in good agreement with the size determined from transmission electron microscopy image (see the superimposed image in Fig. 1a). The saturation magnetization of $M_s = 295$ kA/m was determined from the measured magnetization curve to calculate the core size and reasonably agreed to the value reported in reference [7] for a 12-nm iron oxide particle. Compared to the M_s of bulk magnetite (from 470 to 515 kA/m), the determined M_s was smaller and could be thought due to the existence of mixed phase of magnetite and maghemite. The existence of the second peak corresponded to a particle size of 6.1 nm was assumed to occur due to the substantial inter-core interaction effect that was not accounted in the static magnetization model.

Figure 2 a depicts the dynamic magnetizations of the iron oxide nanoparticles in the carrier liquids having different wt/V % of glycerol. The peaks of the imaginary part of the dynamic magnetization reflected the Brownian relaxation process of the thermally blocked iron oxide nanoparticle where their positions shifted to a lower frequency as the wt/V % of the glycerol increased in the carrier liquids. The thermally blocked particle could be resulted from the presence of the hysteresis in the magnetization [18] where it was also reported in [7] for a 12-nm iron oxide particle. The response showed that the viscosity of the carrier liquid was increased due to the Brownian relaxation mechanism. The peak position of the imaginary part around 400 Hz agreed with the result reported in reference [27]. Using 0.89 mPa s as the viscosity of the purified water (0 wt/V % solution) at 25 °C, the distribution of D_H was determined based on the nonlinear curve fitting of Eq. (4) in the least-squares sense. The solid line shows the constructed hydrodynamic size distribution in Fig. 2 b, where an average diameter of 130 nm, the standard deviation of

Fig. 1 a The static magnetization of the multi-core iron oxide nanoparticles. b The constructed distribution of magnetic moment



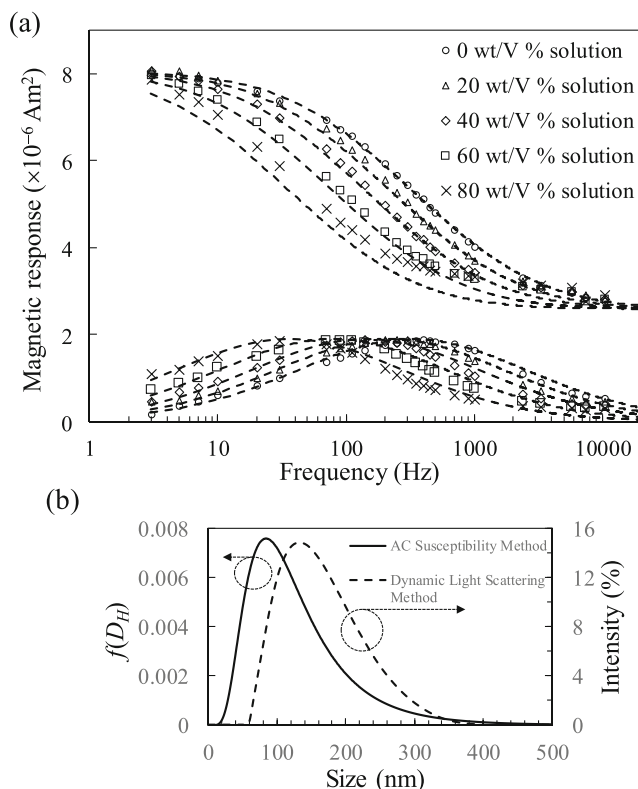


Fig. 2 **a** The real and imaginary parts of dynamic magnetization in different viscosity of carrier liquids. **b** The constructed distributions of hydrodynamic diameter from AC susceptibility and DLS methods

76 nm, and $\langle \sigma \rangle$ of 3.1 were obtained. The comparison between hydrodynamic diameter obtained from the dynamic magnetization and intensity weighted distribution measured using the dynamic light scattering (DLS) method (Zetasizer Nano S90, Malvern Instruments, Worcestershire, UK) is shown as the solid and dashed lines as indicated in Fig. 2 b. The DLS measurement had resulted in a Z-average of 128.7 nm; however, it should be noted that the intensity weighted distribution may overestimate the size due to domination of a few large particles, i.e., the intensity is proportional to D_H^6 [15].

3.2 The Effect of Viscosity on the Dynamics of Particles

The dashed lines in Fig. 2 a show the real and imaginary parts derived from the hydrodynamic diameter distribution. The response indicates a good agreement with the measured data. Since the viscosity of the carrier liquid reflects the peak position of the imaginary part, we estimated the viscosity of the 20 to 80 wt/V % solutions by fitting their imaginary parts with Eq. (5). Here, the previously determined hydrodynamic diameter distribution of the 0 wt/V % solution was used in the nonlinear curve fitting. The dashed lines in Fig. 2 a show the derived for both real and imaginary parts with their corresponding viscosities are plotted in Fig. 3.

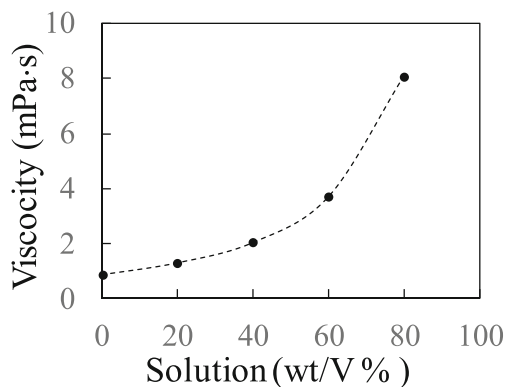


Fig. 3 Estimated viscosity of the carrier liquids with respect to wt/V % of glycerol in the carrier liquids

The derivation results obtained from imaginary parts are in good agreement with the measured data while a slight deviation of the real parts was observed, particularly for the 80 wt/V % solution. This deviation was thought due to the existence of the σ distribution and further clarification on the effect should be investigated.

In practice, measurements that requiring sweeping of a wide range of frequency region result to increment of measuring time. The results indicated that for the change of the real and imaginary parts, a single-frequency measurement could be used to obtain the concentration of MNPs and environmental factors that affected the dynamic magnetization of MNP such as the viscosity of the carrier liquid [28]. The selection of the measurement frequency is crucial, depending on the types of relaxation mechanism. In this work, we selected a frequency of 30 Hz since a lower frequency can capture the information of the Brownian relaxation process occurred at a higher frequency owing to the distribution of the particle size. Figure 4 shows the intensity profile of the first, third, and fifth harmonics of the iron oxide nanoparticle with respect to the viscosity at different intensities of the AC excitation field. Generally, the intensity of the harmonics decreased with the increase of viscosity, which was consistent with the results indicated in Fig. 2 a. Moreover, the intensity of the harmonics increased with the magnitude of the excitation field. However, it should be noted that the increment in the harmonic intensity profile is correlated with the increase in the MNPs concentration, i.e., a slight difference in concentrations of MNPs may result to a negligible difference in harmonic intensity, resulting to an estimation error of the viscosity. This can be shown by the first harmonic during the excitation field of 7.8 mT. On the other hand, the phase angle of the harmonics reflects the phase change of the Brownian relaxation process. In this case, Fig. 5 shows the phase angle change of the harmonics referenced at the phase angle of 0 wt/V % solution (viscosity of 0.89 mPa.s). The phase delay of the harmonics is increased with the increase of the viscosity, which was consistent with the increasing magnitude of the imaginary part in Fig. 2 a.

Fig. 4 **a** The intensity of the first f_1 , **b** third f_3 , and **c** fifth f_5 harmonics concerning viscosity and excitation field

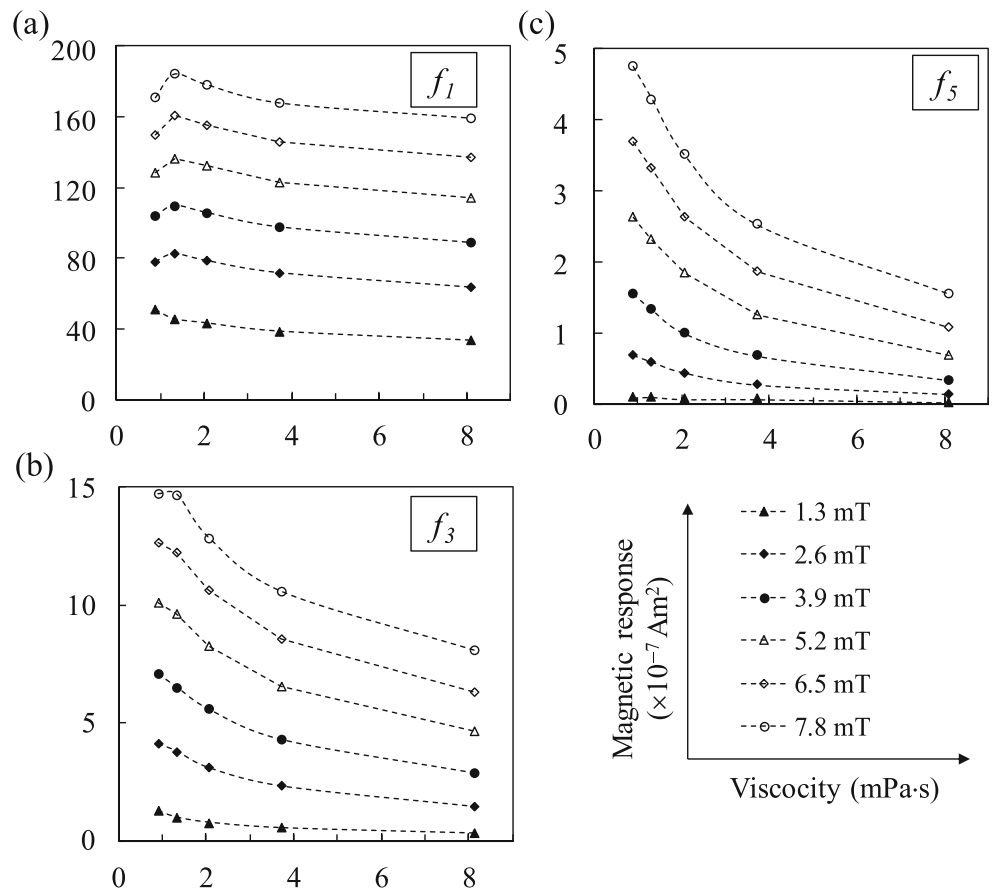


Fig. 5 **a** The phase angle of the first f_1 , **b** third f_3 , and **c** fifth f_5 harmonics concerning viscosity and excitation field

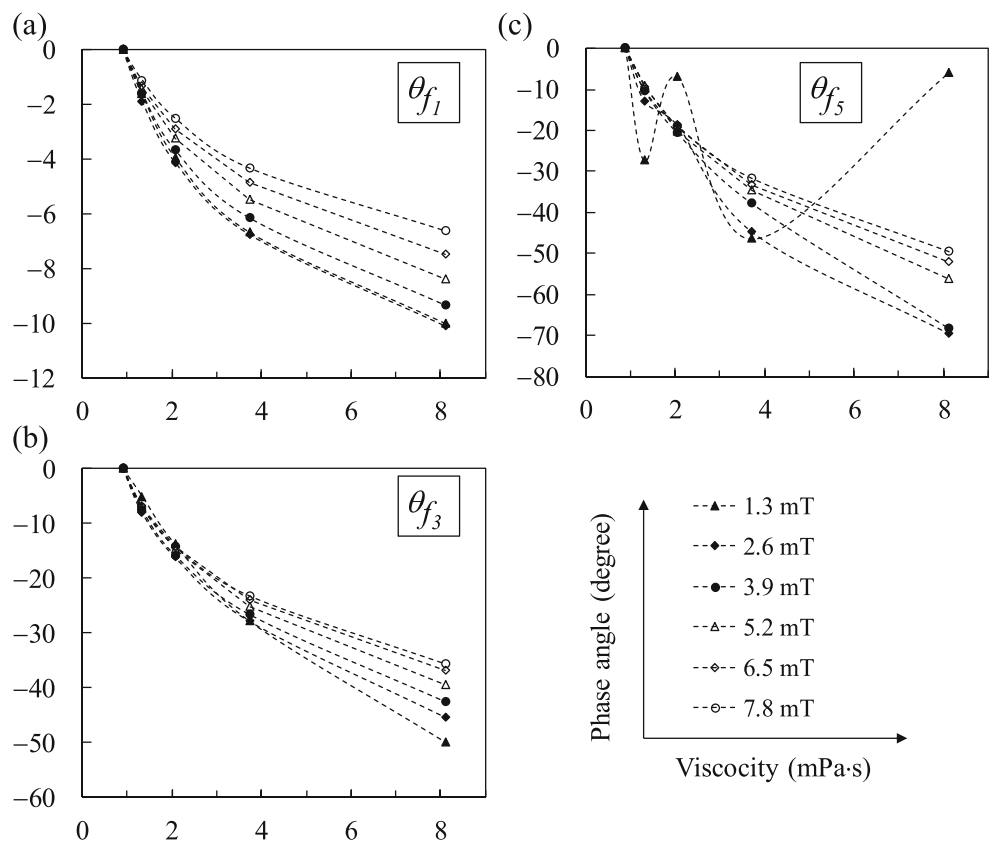
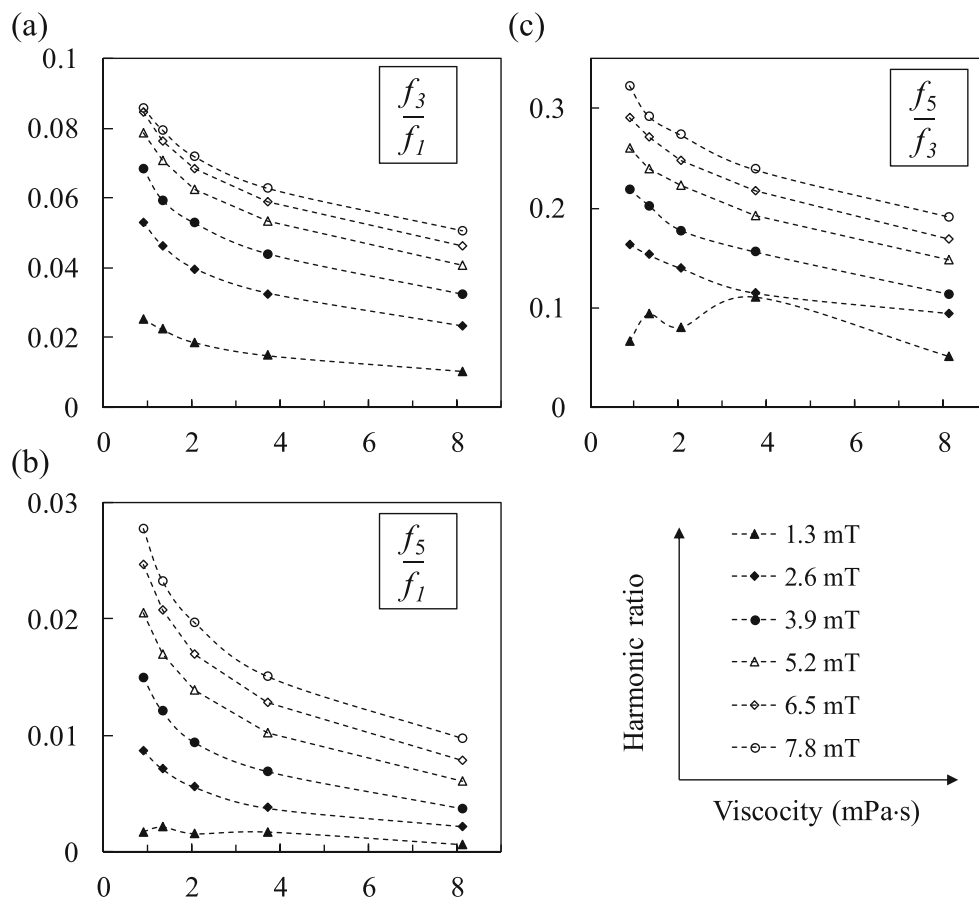


Fig. 6 **a** The harmonics ratio of the f_3/f_1 , **b** f_5/f_1 , and **c** f_5/f_3 with respect to viscosity and excitation field



However, the phase delay was reduced at a higher magnitude of the excitation field. The phenomenon can be interpreted as the higher intensity of magnetic field has increased the magnetic torque of the thermally blocked particles where it reduces the relaxation time, thus resulting in the reduced phase delay. At this point, the viscosity of liquid carrier could be determined quantitatively based on the MNP solution phase angle profile using a known distribution of the hydrodynamic diameter. However, it must be noted that the phase delay is sensitive to the noise when the harmonics intensity is relatively small and comparable to the noise. The condition is shown by the phase angle of the fifth harmonic at the excitation field of 1.3 mT_{pp} in Fig. 5 c. It is known that the intensity of the harmonics is proportional to the concentration of MNPs. By taking a ratio between harmonics, the effect of concentration can be normalized, thus providing a rather simple determination of viscosity using harmonics ratio compared to determination of phase delay. Figure 6 shows the third-to-first, fifth-to-first, and fifth-to-third ratios as a function of the viscosity. The harmonics ratio decreased with the increase of the viscosity. Since high magnetic field will produce a higher harmonics intensity, the harmonics ratio will also increase when the intensity of the excitation field is increased. However, it shall be noted that the phase delay and harmonic

ratio were not linear and depended on the strength of the AC magnetic field. Therefore, it can be proved that harmonics ratio can be used as a concentration-independent parameter in the determination of the MNP's dynamics.

4 Conclusion

The static and dynamic magnetizations of the multi-core iron oxide nanoparticles have been characterized by the developed systems. The core size of 11.7 nm and its hydrodynamic diameter profile with an average diameter of 130 nm derived from their static and dynamic magnetizations were consistent with the results achieved by TEM analysis and DLS measurement. It is indicated that the environmental factors such as viscosity could affect the dynamic behavior of MNPs where the peaks of the imaginary components shifted to a lower frequency region when the solution viscosity was increased from 0.89 to 8.11 mPa s. Also, it was shown that the harmonic ratio decreased and the phase angle delay increased when the viscosity was increased. The harmonics ratio and phase angle delay could be used as the concentration-independent parameter to estimate the viscosity of the

liquid carrier where it can be implemented in certain applications such as in the magnetic immunoassay and magnetic particle imaging (MPI) technique.

Funding Information This work was supported by the Ministry of Higher Education of Malaysia under grant number of RDU 160115, Research Management Center of Universiti Malaysia Pahang under grant number of RDU 170377, and the “Strategic Promotion of Innovative R&D” of the Japan Science and Technology Agency (JST).

Publisher’s Note Springer Nature remains neutral with regard to jurisdictional claims in published maps and institutional affiliations.

References

- Saritas, E.U., Goodwill, P.W., Croft, L.R., Konkle, J.J., Lu, K., Zheng, B., Conolly, S.M.: Magnetic particle imaging (MPI) for NMR and MRI researchers. *J. Magn. Reson.* **229**, 116–126 (2013). <https://doi.org/10.1016/j.jmr.2012.11.029>
- Gleich, B., Weizenecker, J.: Tomographic imaging using the non-linear response of magnetic particles. *Nature.* **435**, 1214–1217 (2005). <https://doi.org/10.1038/nature03808>
- Goodwill, P.W., Scott, G.C., Stang, P.P., Conolly, S.M.: Narrowband magnetic particle imaging. *IEEE Trans. Med. Imaging.* **28**, 1231–1237 (2009). <https://doi.org/10.1109/TMI.2009.2013849>
- Bai, S., Hirokawa, A., Tanabe, K., Sasayama, T., Yoshida, T., Enpuku, K.: Narrowband magnetic particle imaging utilizing electric scanning of field free point. *IEEE Trans. Magn.* **51**, 1–4 (2015). <https://doi.org/10.1109/TMAG.2015.2438029>
- Vogel, P., Rückert, M.A., Klauer, P., Kullmann, W.H., Jakob, P.M., Behr, V.C.: First in vivo traveling wave magnetic particle imaging of a beating mouse heart. *Phys. Med. Biol.* **61**, 6620–6634 (2016). <https://doi.org/10.1088/0031-9155/61/18/6620>
- Graeser, M., Knopp, T., Swargulski, P., Friedrich, T., von Gladiss, A., Kaul, M., Krishnan, K.M., Itrich, H., Adam, G., Buzug, T.M.: Towards picogram detection of superparamagnetic Iron-oxide particles using a gradiometric receive coil. *Sci. Rep.* **7**, 6872 (2017). <https://doi.org/10.1038/s41598-017-06992-5>
- Ozel, F., Kockar, H., Karaagac, O.: Growth of iron oxide nanoparticles by hydrothermal process: effect of reaction parameters on the nanoparticle size. *J. Supercond. Nov. Magn.* **28**, 823–829 (2015). <https://doi.org/10.1007/s10948-014-2707-9>
- Connord, V., Mehdaoui, B., Tan, R.P., Carrey, J., Respaud, M.: An air-cooled Litz wire coil for measuring the high frequency hysteresis loops of magnetic samples - a useful setup for magnetic hyperthermia applications. *Rev. Sci. Instrum.* **85**, 093904 (2014). <https://doi.org/10.1063/1.4895656>
- Mamiya, H., Jeyadevan, B.: Hyperthermic effects of dissipative structures of magnetic nanoparticles in large alternating magnetic fields. *Sci. Rep.* **1**, 157 (2011). <https://doi.org/10.1038/srep00157>
- Enpuku, K., Tanaka, T., Matsuda, T., Dang, F., Enomoto, N., Hojo, J., Yoshinaga, K., Ludwig, F., Ghaffari, F., Heim, E., Schilling, M.: Properties of magnetic nanoparticles in the Brownian relaxation range for liquid phase immunoassays. *J. Appl. Phys.* **102**, 054901 (2007). <https://doi.org/10.1063/1.2775882>
- Calero-DdelC, V.L., Santiago-Quifonez, D.I., Rinaldi, C.: Quantitative nanoscale viscosity measurements using magnetic nanoparticles and SQUID AC susceptibility measurements. *Soft Matter.* **7**, 4497 (2011). <https://doi.org/10.1039/c0sm00902d>
- Karaagac, O., Kockar, H.: A simple way to obtain high saturation magnetization for superparamagnetic iron oxide nanoparticles synthesized in air atmosphere: optimization by experimental design. *J. Magn. Magn. Mater.* **409**, 116–123 (2016). <https://doi.org/10.1016/j.jmmm.2016.02.076>
- Ludwig, F., Balceris, C., Jonasson, C., Johansson, C.: Analysis of ac susceptibility spectra for the characterization of magnetic nanoparticles. **9464** (2017). <https://doi.org/10.1109/TMAG.2017.2693420>
- Ludwig, F., Heim, E., Schilling, M.: Characterization of superparamagnetic nanoparticles by analyzing the magnetization and relaxation dynamics using fluxgate magnetometers. *J. Appl. Phys.* **101**, 113909 (2007). <https://doi.org/10.1063/1.2738416>
- Bogren, S., Fornara, A., Ludwig, F., del Puerto Morales, M., Steinhoff, U., Hansen, M., Kazakova, O., Johansson, C.: Classification of magnetic nanoparticle systems—synthesis, standardization and analysis methods in the nanomag project. *Int. J. Mol. Sci.* **16**, 20308–20325 (2015). <https://doi.org/10.3390/ijms160920308>
- Sasayama, T., Yoshida, T., Saari, M.M.M., Enpuku, K.: Comparison of volume distribution of magnetic nanoparticles obtained from M-H curve with a mixture of log-normal distributions. *J. Appl. Phys.* **117**, 17D155 (2015). <https://doi.org/10.1063/1.4919268>
- Berkov, D.V., Görmert, P., Buske, N., Gansau, C., Mueller, J., Giersig, M., Neumann, W., Su, D.: New method for the determination of the particle magnetic moment distribution in a ferrofluid. *J. Phys. D: Appl. Phys.* **33**, 331–337 (2000). <https://doi.org/10.1088/0022-3727/33/4/303>
- Saari, M.M., Sakai, K., Kiwa, T., Sasayama, T., Yoshida, T., Tsukada, K.: Characterization of the magnetic moment distribution in low-concentration solutions of iron oxide nanoparticles by a high- T_c superconducting quantum interference device magnetometer. *J. Appl. Phys.* **117**, 17B321 (2015). <https://doi.org/10.1063/1.4919043>
- Suhaimi, N.S., Saari, M.M., Mohamed, A.I., et al.: Development of a compact and sensitive AC magnetometer for evaluation of magnetic nanoparticles solution. In: 2017 IEEE 8th Control and System Graduate Research Colloquium (ICSGRC). IEEE, pp 221–224 (2017)
- Shliomis, M.I., Stepanov, V.I.: Frequency dependence and long time relaxation of the susceptibility of the magnetic fluids. *J. Magn. Magn. Mater.* **122**, 176–181 (1993). [https://doi.org/10.1016/0304-8853\(93\)91067-H](https://doi.org/10.1016/0304-8853(93)91067-H)
- Saari, M.M., Suhaimi, N.S., Razali, S., et al.: Development of a resonant excitation coil of AC magnetometer for evaluation of magnetic fluid. *J. Telecommun Electron Comput Eng.* **10**, 127–130 (2018)
- Svedlindh, P., Jonsson, T., García-Palacios, J.L.: Intra-potential-well contribution to the AC susceptibility of a noninteracting nano-sized magnetic particle system. *J. Magn. Magn. Mater.* **169**, 323–334 (1997). [https://doi.org/10.1016/S0304-8853\(96\)00756-1](https://doi.org/10.1016/S0304-8853(96)00756-1)
- Ludwig, F., Balceris, C., Johansson, C.: The anisotropy of the AC susceptibility of immobilized magnetic nanoparticles—the influence of intra-potential-well contribution on the AC susceptibility spectrum. *IEEE Trans. Magn.* **53**, 1–4 (2017). <https://doi.org/10.1109/TMAG.2017.2692038>
- Enpuku, K., Sasayama, T., Yoshida, T.: Estimation of magnetic moment and anisotropy energy of magnetic markers for biosensing application. *J. Appl. Phys.* **119**, 184902 (2016). <https://doi.org/10.1063/1.4948951>
- Prieto Astalan, A., Jonasson, C., Petersson, K., Blomgren, J., Ilver, D., Krozer, A., Johansson, C.: Magnetic response of thermally blocked magnetic nanoparticles in a pulsed magnetic field. *J. Magn. Magn. Mater.* **311**, 166–170 (2007). <https://doi.org/10.1016/j.jmmm.2006.10.1182>

26. van Rijssel, J., Kuipers, B.W.M., Ern , B.H.: Non-regularized inversion method from light scattering applied to ferrofluid magnetization curves for magnetic size distribution analysis. *J. Magn. Mater.* **353**, 110–115 (2014). <https://doi.org/10.1016/j.jmmm.2013.10.025>
27. Ahrentorp, F., Astalan, A.P., Jonasson, C., et al.: Sensitive high frequency AC susceptometry in magnetic nanoparticle applications. *AIP Conf Proc.* **1311**, 213–223 (2010). <https://doi.org/10.1063/1.3530015>
28. Rauwerdink, A.M., Weaver, J.B.: Harmonic phase angle as a concentration-independent measure of nanoparticle dynamics. *Med. Phys.* **37**, 2587–2592 (2010). <https://doi.org/10.1118/1.3426294>